

Directed-loop Monte Carlo simulations of vertex models

Olav F. Syljuåsen¹ and M. B. Zvonarev²

¹*NORDITA, Blegdamsvej 17, Copenhagen Ø, DK-2100 Denmark*^{*}

²*Ørsted Laboratory, Niels Bohr Institute for APG,
Universitetsparken 5, Copenhagen Ø, DK 2100, Denmark*[†]

(Dated: January 13, 2019)

We show how the directed-loop Monte Carlo algorithm can be applied to study vertex models. The algorithm is employed to calculate the arrow polarization in the six-vertex model with the domain wall boundary conditions (DWBC). The model exhibits spatially separated ordered and “disordered” regions. We show how the boundary between these regions depends on parameters of the model. We give some predictions on the behavior of the polarization in the thermodynamic limit and discuss the relation to the Arctic Circle theorem.

PACS numbers: 05.10.Ln, 05.50.+q, 02.30.Ik

I. INTRODUCTION

Vertex models have a long and distinguished history in physics. Their fame is intimately connected to the concept of integrability, and the exact solutions of the six-vertex [1] and the eight-vertex [2] models with periodic boundary conditions (PBC) are indeed milestones in physics. Despite being exactly solvable, there are questions about these models that cannot easily be answered. An example is the influence of boundary conditions on correlation functions. While boundary conditions are not normally important in the thermodynamic limit, they have a profound influence on the vertex models. Exact studies, made for the six-vertex model with the domain wall boundary conditions (DWBC) [3] show this in particular. These studies were restricted to certain points in the phase diagram, and involve rather sophisticated mathematical methods. It is thus appropriate to complement them with Monte Carlo simulations.

The purpose of this article is to demonstrate that the directed-loop Monte Carlo algorithm developed for quantum spin systems [4] can be used as a tool to study vertex models. The discussion of the algorithm will be kept general, but when demonstrating its use we will focus on the six-vertex model with the DWBC, a model which is difficult to simulate using other known Monte Carlo algorithms.

II. MONTE CARLO ALGORITHM

In a vertex model, each vertex have edges with an Ising-like variable, an arrow, that points either away from or into the vertex. The arrangement of arrows around the vertex determines the vertex weight. Two vertices are joined by their common edge, sharing the arrow on the edge. In general there are no restrictions on which

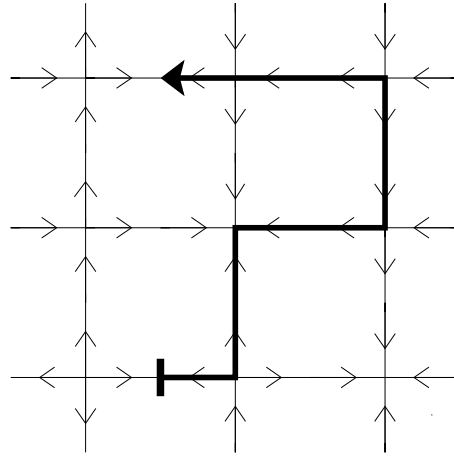


FIG. 1: Illustration of the directed-loop algorithm. Vertex edges are drawn with two arrows allowing the discontinuity at the head and tail of the loop to be shown. The thick line shows the loop path along which the arrows has been flipped. The loop closes when the loop head (thick arrow) hits the loop tail (vertical bar).

vertices are joined, however for traditional vertex models nearest-neighbor vertices are joined together. The Monte Carlo algorithm discussed here always flips two (or zero) arrows on a vertex, thus it is limited to models where an even number of arrows are pointing away from each vertex. Most vertex models of interest obey this rule.

In visualizing the directed-loop Monte Carlo algorithm, originally developed for quantum systems [4], it is helpful to cut every edge into two pieces, each piece having an arrow belonging to a specific vertex, Fig. 1. For a valid vertex configuration the arrows on the two parts of an edge must have the same orientation. The directed-loop algorithm is as follows: Pick a random vertex v_1 and a random edge belonging to that vertex. Based on these choices select in a probabilistic manner another edge belonging to v_1 and name that the out-edge. Then flip the arrows on both the part of the in-edge and the part of the out-edge belonging to v_1 . This introduces two discontinuities in the arrow configurations on the edges, one on

^{*}Electronic address: sylju@nordita.dk

[†]Electronic address: zvonarev@fys.ku.dk

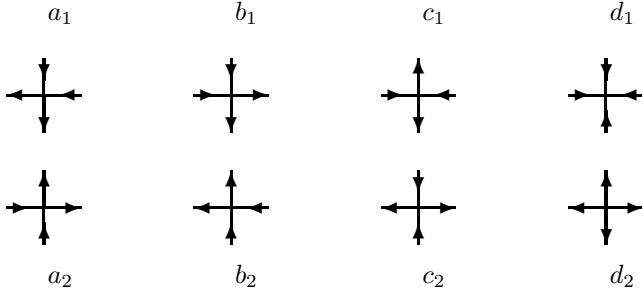


FIG. 2: The vertices of the eight-vertex model and their statistical weights.

the starting in-edge and another one on the out-edge. The new configuration is thus not an allowed vertex configuration. To repair this, the out-edge discontinuity is moved by repeating the procedure on the vertex connected to the out-edge v_2 , this time using the out-edge of v_1 and the in-edge on v_2 . The process is stopped when the out-edge selected is the starting edge, thus healing all discontinuities. In this way arrows are flipped as a loop is constructed, and a new allowed vertex configuration is arrived at when the loop closes.

In order to determine the probabilities for selecting out-edges and to see how detailed balance is satisfied one needs to consider also the probability for the reverse update. The reverse update consists of traversing the same loop in the opposite direction while flipping arrows back. As is explained in detail in Ref. [4], detailed balance is satisfied for the whole loop construction, if detailed balance is satisfied in each edge selecting step, for which the criterion is as follows: Let w be the weight of the vertex v before edge-flips, then the probability $P(v, i \rightarrow o)$ for exiting at the out-edge o , given that the in-edge is i , should satisfy

$$wP(v, i \rightarrow o) = w'P(v', o \rightarrow i), \quad (1)$$

where w' is the weight of the vertex v' obtained by flipping the arrows on edges i and o belonging to the vertex v . Notice that $P(v', o \rightarrow i)$, on the right hand side, describes an edge-selecting step in the reverse update process where the loop is traversed in the opposite direction to that described on the left hand side. The loop construction should not terminate in the edge-selecting step, thus

$$\sum_o P(v, i \rightarrow o) = 1, \quad (2)$$

where the sum is taken over all possible out-edges, including the in-edge i .

This algorithm is very similar to the long loop algorithm of Barkema and Newman [5]. In fact, at the point in parameter space where all vertex weights are equal the two algorithms are identical. However away from this point, Barkema and Newman's algorithm involves accepting or rejecting the loop after it has been

constructed. The directed-loop algorithm has no such accept/reject step.

The Eqs. (1) and (2) form several coupled sets which in most cases are under-determined. There are thus many solutions for the out-edge selection probabilities P . Some general solutions and analysis of their efficiency for different quantum systems were reported in Ref. [6]. Here we employ the solution B in Ref. [6] to the eight-vertex model, but solutions for higher-vertex models are not hard to find as well. The allowed vertices for the eight-vertex model and their statistical weights are shown in Fig. 2. To shorten notation, we consider the so-called symmetric case: the statistical weights, a, b, c , and d , of the allowed states are assumed to be invariant under the simultaneous reversal of all arrows. The generalization of the algorithm to the non-symmetric case can be performed easily.

Let W_1, \dots, W_4 be the vertex weights a, b, c, d of the eight-vertex model ordered so that $W_1 \geq W_2 \geq W_3 \geq W_4$. Then the probability for picking the out-edge on a vertex with weight W_i resulting in a new vertex weight W_j after flipping arrows is t_{ij}/W_i , where $t_{ij} = t_{ji}$ and the non-zero entries of the 4×4 matrix t are

$$\begin{aligned} t_{12} &= (W_1 + W_2 - W_3 - W_4)/2, \\ t_{13} &= (W_1 - W_2 + W_3 - W_4)/2, \\ t_{23} &= (-W_1 + W_2 + W_3 + W_4)/2, \\ t_{14} &= W_4, \end{aligned} \quad (3)$$

when $W_1 - W_2 - W_3 - W_4 \leq 0$. Otherwise one needs to include bounces in which the out-edge coincides with the in-edge. In this case a solution can be chosen as follows:

$$\begin{aligned} t_{11} &= W_1 - W_2 - W_3 - W_4, \\ t_{1j} &= t_{j1} = W_j, \quad j = 2, 3, 4, \\ t_{ij} &= 0, \quad \text{otherwise.} \end{aligned} \quad (4)$$

The algorithm presented here has many similar features to the loop algorithm [7]. However the equation sets arrived at in the loop algorithm have a more restricted set of solutions for vertices with many edges. For the eight-vertex model these restrictions are alleviated by freezing loops together. The similar feature here is the bounce process. The need for bounces is generally not so crucial for higher-vertex models with many weights of the same magnitude, thus we expect that the directed-loop algorithm should work well in simulating higher-vertex models.

Note also that an algorithm based on the directed-loop idea was recently demonstrated to be effective in simulating classical integer-valued link-current models [8].

III. SIX-VERTEX MODEL WITH THE DWBC

The six-vertex model with the DWBC was introduced in Ref. [9] in connection with the calculation of the correlation functions for exactly solvable $1+1$ dimensional

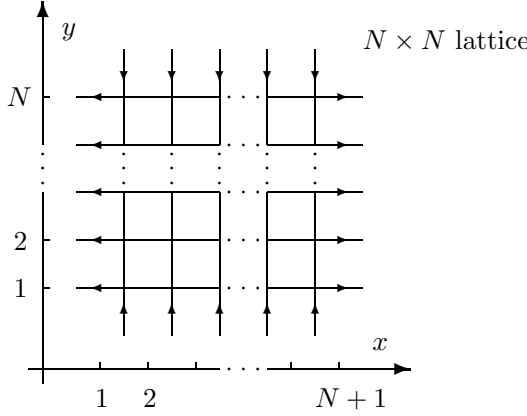


FIG. 3: The domain wall boundary conditions. Shown is an $N \times N$ lattice. The total number of vertices is N^2 . The coordinates label horizontal edges.

models [3]. Here we recall the definition of the model in brief, referring for further details to the Ref. [10] where a more detailed description of the model and a comprehensive list of references are given.

The model is defined on an $N \times N$ square lattice; the thermodynamic limit corresponds to $N \rightarrow \infty$. There are six possible states at each vertex: one should set $d = 0$ in the eight-vertex model defined above, Fig. 2. The model is symmetric: the statistical weights, a , b , and c , of the allowed states are assumed to be invariant under the simultaneous reversal of all arrows. Hence, the model is characterized by only two parameters, which can be taken to be a/c and b/c . We set $c = 1$ henceforth.

The DWBC imply that all arrows on the top and bottom of the lattice are pointing inward, while all arrows on the left and right boundaries are pointing outward, Fig. 3.

In the simulation vertices belonging to the boundary are treated differently from the bulk vertices. In the bulk one finds by setting $d = W_4 = 0$ and $c = 1$ in Eqs. (3), that bounces are only necessary when $a+b < 1$ or $|a-b| > 1$. For the boundary vertices the loop is not allowed to exit on the boundary edges, because the arrows on these edges are fixed by the boundary conditions. This leads to more restricted equation sets (many W 's are equal to zero) for the boundary vertices and generally requires the inclusion of bounce processes.

To investigate the spatially inhomogeneous behavior of this model we focus on the polarization, $\chi_N(x, y)$ [10, 11], which is the ensemble average of the arrow direction on the edge with coordinates (x, y) on the $N \times N$ lattice. The symmetry of the model allows us to consider only arrows on the horizontal edges. The value $+1$ (-1) is assigned to an arrow pointing to the right (left). The coordinate system used is shown in Fig. 3.

Obviously, χ_N is independent of the coordinates of the edge in case of PBC. For these boundary conditions χ_N is known in the thermodynamic limit, and exhibits fer-

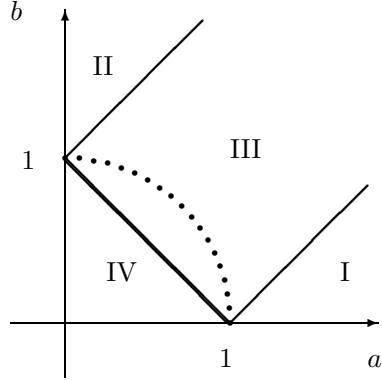


FIG. 4: The phase diagram in terms of the weights a and b .

roelectric order, antiferroelectric order or no order, depending on the position on the (a, b) plane. Thus, three phases exist in the six-vertex model with PBC: ferroelectric, antiferroelectric, and disordered phase. In Fig. 4 the phase diagram on the (a, b) plane for the model with PBC is plotted (cf., Fig. 8.5 of Ref. [2]).

Introduce a parameter Δ by the formula

$$\Delta = \frac{a^2 + b^2 - 1}{2ab}. \quad (5)$$

The case $\Delta > 1$ (regions I and II in Fig. 4) corresponds to the ferroelectric phase; the case $-1 < \Delta < 1$ (region III in Fig. 4) to the disordered phase; the case $\Delta < -1$ (region IV in Fig. 4) to the antiferroelectric phase.

Fig. 4 may be considered as the phase diagram for the model with the DWBC, in the sense that the free energy takes a different analytic form in the regions I through IV (see Ref. [12] for details). But, in case of the DWBC the polarization χ_N depends on the position of the edge. In the next section we show numerical results for χ_N on horizontal edges as the parameters a and b are varied.

IV. RESULTS

(i) Disordered phase: $-1 < \Delta < 1$. First consider the particular case $\Delta = 0$ (dotted quartercircle in Fig. 4). An exact expression for $\chi_N(x, y)$ in this case was obtained by Kapitonov and Pronko [13] recently. To check our algorithm we have compared results for the polarization at the point $a = b = 1/\sqrt{2}$ with the exact results of Ref. [13]. The comparison can be seen in Fig. 5, where the polarization is shown as a function of x for different values of y and system sizes, N . One can clearly see that the boundary values of the polarization, ± 1 , extends a finite distance into the bulk. This distance depends on y and is larger at the upper and lower boundaries. The areas where the polarization stays at its boundary values are termed “frozen” regions. Going further into the bulk, there is a transition to a “disordered” region, where apart

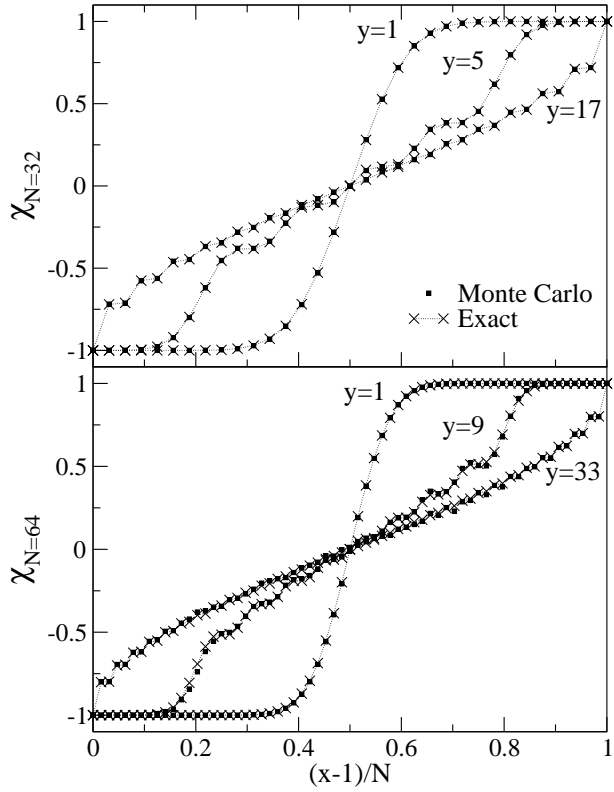


FIG. 5: Horizontal polarization as a function of x for different values of y . Results for two different system sizes are shown: $N = 32$ (upper panel) and $N = 64$ (lower panel). The filled symbols are Monte Carlo results, while the crosses are exact results gotten from Ref. [13]. The dotted lines are guides to the eye.

from small wiggles due to the finite system size, the polarization changes smoothly. It is interesting to note that there never is any extended regime where the polarization is zero, as is the case for PBC. The transition between the “frozen” and “disordered” regions gets sharper as the system size is increased, as can be seen by comparing the two panels in Fig. 5.

It is convenient to visualize the behavior of the polarization using greyscale plots, where greyvalues are assigned to values of $\chi_N(x, y)$ and each point corresponds to a horizontal edge following the layout described in Fig. 3. For $a = b = 1/\sqrt{2}$ such a plot is shown in Fig. 6.(a). The four “frozen” corners are clearly apparent. In these regions, the vertices are all of the same type, and are, from upper left to bottom right, a_1, b_1, b_2, a_2 , respectively. To measure the area of the “frozen” regions, we define a threshold value $\epsilon = 0.08$, such that points (x, y) where $|\chi_N(x, y)| > 1 - \epsilon$ are judged to be in a “frozen” region. Applying this we find that each “frozen” corner is 4.6% of the total area. This value changes relatively little changing the value of ϵ .

Going away from the $\Delta = 0$ curve, let us follow along the diagonal, $a = b$, towards $\Delta = \infty$ first, Fig. 6. As the values of the vertex weights a and b increase, the

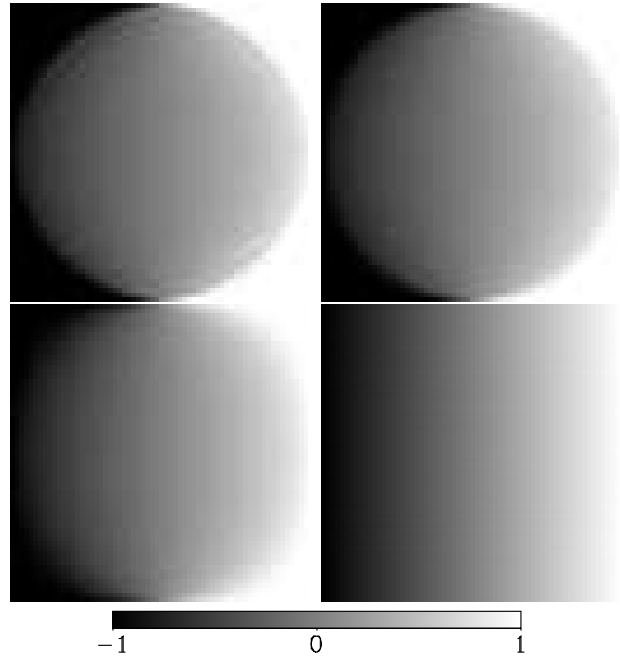


FIG. 6: Greyscale plot of the polarization $\chi_N(x, y)$ for $N = 64$ and (from upper left to bottom right) $a = b = 1/\sqrt{2}, 1, 3, 100$.

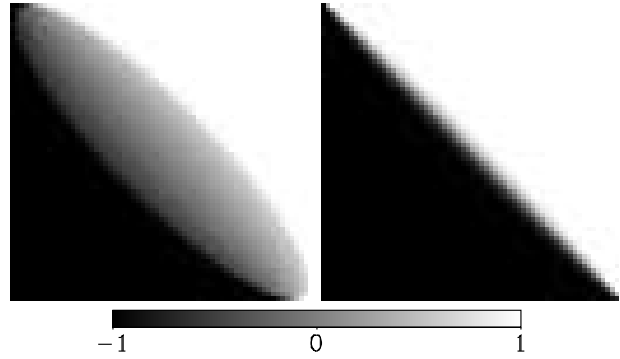


FIG. 7: Greyscale plot of the polarization $\chi_N(x, y)$ for $N = 64$, $a = 0.25$ and, from left to right, (a) $b = \sqrt{15/16}$ (b) $b = 1.25$

area of the “frozen” regions decreases. We find that with $\epsilon = 0.08$ each frozen corner in (b) is 4.0% of the total area, and 2.8% in (c). For very high values of $a = b$, the polarization $\chi_N(x, y)$ increases linearly from -1 to 1 as x goes from 0 to 1 , independent of y , as can be seen in Fig. 6 (d). This is consistent with what is expected from an ensemble of configurations with the smallest possible number of c -type vertices: $N!$ configurations each with a single c -type vertex on every row and column.

Consider now $a \neq b$. Because of the symmetry of the phase diagram, Fig. 4, one can choose $b > a$ without loss of generality. The weights of the vertices in the four “frozen” corners are no longer equal, and the “dis-

ordered" region distorts into an oblong shape oriented along the diagonal with large corners of b_2 and b_1 vertices, see Fig. 7. The simulations for $a = 0.25$, $b = \sqrt{15}/16$ ($\Delta = 0$) are shown in Fig. 7(a). The width of the oblong region shrinks as b increases keeping a fixed, $a = 0.25$, and becomes very thin at the boundary to the ferroelectric region, as can be seen in Fig. 7(b). Along this boundary, $b = a + 1$, the width of the oblong region expands as a increases with N being constant.

(ii) Antiferroelectric phase: $\Delta < -1$. The simulations in the antiferroelectric phase are less efficient than in the disordered phase. This is partly due to the presence of the bounce processes also for bulk vertices, but another feature which makes the simulations difficult in this phase is the degeneracy of the two types of antiferroelectric orders. In the antiferroelectric phase it becomes energetically favorable to have a maximum amount of c -type vertices which is achieved by placing c -type vertices in a diamond placed in the center of the lattice. For an even N this diamond can be placed in two equivalent places differing only by one lattice spacing. The Monte Carlo algorithm is however slow in tunneling between these configurations, and this sets a limit to its performance. For odd N there is no such a degeneracy and the simulations are more efficient. Greyscale plots of the polarization for $a = b = 0.5$ and $a = b = 0.375$ are shown in Fig. 8. We have plotted results for both even and odd N . One can see that the "disordered" region approaches a diamond-like shape as $a = b$ decreases ($\Delta \rightarrow -\infty$), compare Figs. 8(a) and (b). For odd N antiferroelectric oscillations are clearly visible in the center of Figs. 8(c) and (d), while they are much weaker for even N , Figs. 8(a) and (b), reflecting the degeneracy mentioned above. For odd N these oscillations are weaker at $a = b = 0.5$ than at $a = b = 0.375$.

For $a \neq b$ greyscale plots are shown in Fig. 9. Here antiferroelectric oscillations in the middle of the plot are visible for $a = 0.25$ and $b = 0.5$, Fig. 9(a) while they have almost vanished at the boundary between the antiferroelectric and disordered phases, Fig. 9(b).

The exact expression is known [10] for the polarization along the boundary, $\chi_N(x, 1)$. Comparing our Monte Carlo data to this expression we find that in no cases is the absolute difference bigger than 0.016, which is comparable to the statistical errors of our simulations.

V. DISCUSSION

We have considered the phase diagram of the model for the given N . Now, discuss the following problem: what happens with $\chi_N(x, y)$ in the thermodynamic limit, $N \rightarrow \infty$? It is natural to expect that differences in the behavior of the polarization in the different parts of the phase plane, Fig 4, become more pronounced as $N \rightarrow \infty$. As one can see in Fig. 5, the wiggles in the "disordered" region decrease with N increasing, and this is, indeed, the case for all the points (a, b) lying in the disordered

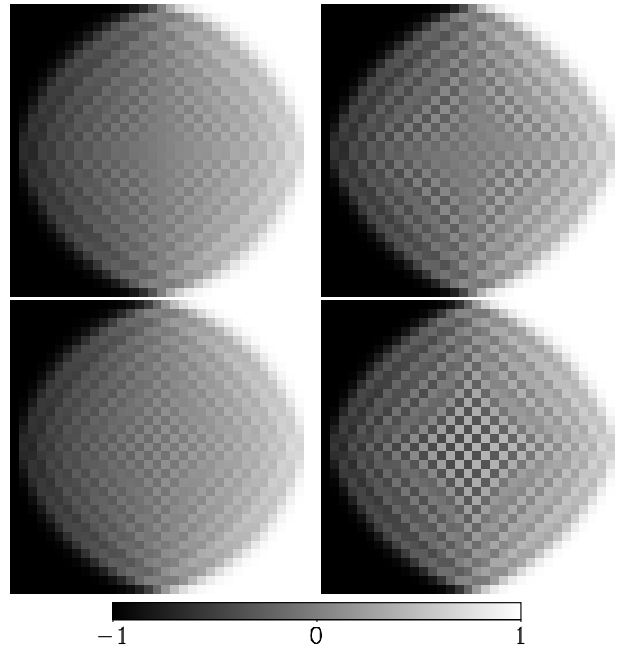


FIG. 8: Greyscale plot of the polarization $\chi_N(x, y)$ for $a = b = 0.5$ (left plots) and $a = b = 0.375$ (right plots). Two different system sizes are shown: $N = 32$ (top) and $N = 33$ (bottom).

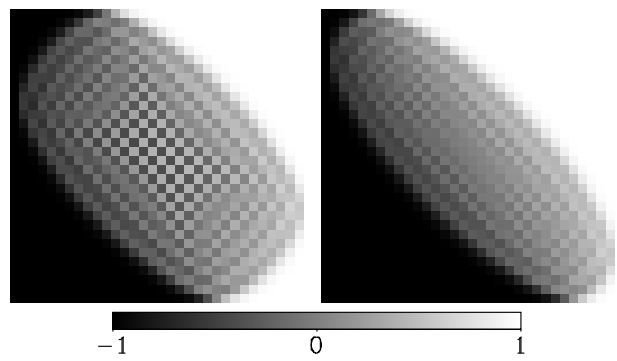


FIG. 9: Greyscale plot of the polarization $\chi_N(x, y)$ for $N = 32$, $a = 0.25$ and, from left to right, (a) $b = 0.5$ (b) $b = 0.75$.

phase and checked in our simulations. We expect that these wiggles, coming from the antiferroelectrically ordered configurations, should vanish completely in the thermodynamic limit for this phase. The next conjecture we want to make is on the behavior of the polarization along the boundary, $\chi_N(x, 1)$. It is known that for $\Delta = 0$, as well as at the point $a = b = 1$, the boundary polarization becomes the Heaviside step function in the thermodynamic limit [10, 14]. We conjecture that this is the case for the whole disordered phase; the position of the discontinuity will depend on the ratio between a and b .

Further, note that for $a = b = 1/\sqrt{2}$ there is a map-

ping (see, *e.g.*, Ref. [12]) of the six-vertex model with the DWBC onto the so-called model of domino tilings of the Aztec diamond. The thermodynamic behavior of the latter model was investigated in Refs. [15]. It shows the same features as in Fig. 6(a): the tilings are ordered (frozen) in the corners of the diamond, while going inside one falls into the “disordered” region. All these features were named the “Arctic Circle Theorem”, since the shape of the boundary between the “frozen” and “disordered” regions is circular. The transition between “frozen” and “disordered” regions is step-like, with the height of the step function depending on the coordinates x and y .

We expect the analogue of the Arctic Circle Theorem to take place for the whole disordered phase: there should be the “frozen” regions, “disordered” region, and a sharp transition between them. We expect also that the profile of the boundary between the “frozen” and “disordered” regions is circular for $a = b$, even though there is no obvious symmetry protecting this statement. Note that the very “smeared” profile in Fig. 6(d) does not contradict our hypotheses because $N = 64$ is relatively small compared to the values of the vertex weights a and b , and is thus far from the thermodynamic limit for this point of the phase diagram.

For the ferroelectric phase, $\Delta > 1$, the profile in Fig. 7 leads to the obvious conjecture: in the whole ferroelectric phase a sharp discontinuity from a “frozen” domain with b_1 vertices to the one with b_2 -vertices takes place in the thermodynamical limit.

To this end, consider the antiferroelectric phase. We expect the step-like behavior of the boundary polarization in this phase in the thermodynamic limit, as well as the existence of the “frozen” regions in the corners.

Our statements on the behavior of the polarization deep inside the lattice are more speculative. For $a = b$ and even N the height of the antiferroelectric oscillations decreases, while for odd N these oscillations seem to be non-vanishing in the large N limit. Our belief is that there is a finite region with antiferroelectric order for odd N , as $N \rightarrow \infty$, while for even N the polarization exhibits no such an order.

Finally, we would like to stress that the directed-loop algorithm can also be applied to study the six-vertex model with any boundary conditions, and the higher-vertex models. These could help in solving the problems for which the analytical methods are difficult to apply. For example, the six-vertex model with any boundary conditions can be considered as a model for a description of interface roughening of a crystal surface [16]. An important point in studies Refs. [16] is the existence of exact analytical results for the six-vertex model with PBC [1, 2]. Therefore, numerical data referring to other boundary conditions than PBC could give a new insight for these studies.

Acknowledgments

We thank V.V. Cheianov and A.G. Pronko for useful discussions and the authors of the work [13] for providing us with their data. M.B. Zvonarev’s work was supported by the Danish Technical Research Council via the Framework Programme on Superconductivity. Monte Carlo calculations were in part carried out using NorduGrid, a Nordic facility for Wide Area Computing and Data Handling.

[1] E.H. Lieb, Phys. Rev. **162**, 162 (1967); Phys. Rev. Lett. **18**, 1046 (1967); **19**, 108 (1967); B. Sutherland, *ibid.* **19**, 103 (1967).

[2] R.J. Baxter, *Exactly Solved Models in Statistical Mechanics* (Academic Press, San Diego, 1982).

[3] V.E. Korepin, N.M. Bogoliubov, and A.G. Izergin, *Quantum Inverse Scattering Method and Correlation Functions* (Cambridge University Press, Cambridge, 1993).

[4] O.F. Syljuåsen and A. Sandvik, Phys. Rev. E, **66**, 046701 (2002).

[5] G.T. Barkema and M.E.J. Newman, Phys. Rev. E **57**, 1155 (1998).

[6] O.F. Syljuåsen, Phys. Rev. E, **67**, 046701 (2003).

[7] H.G. Evertz, G. Lana and M. Marcu, Phys. Rev. Lett. **70**, 875 (1993).

[8] F.Alet and E.S. Sørensen, Phys. Rev. E, **68**, 026702 (2003).

[9] V.E. Korepin, Commun. Math. Phys. **86**, 391 (1982).

[10] N.M. Bogoliubov, A.G. Pronko, and M.B. Zvonarev, J. Phys. A **35**, 5525 (2002).

[11] N.M. Bogoliubov, A.V. Kitaev, and M.B. Zvonarev, Phys. Rev. E, **65**, 026126 (2002).

[12] P. Zinn-Justin, Phys. Rev. E **62**, 3411 (2000).

[13] V.S. Kapitonov and A.G. Pronko, *private communication*.

[14] D. Zeilberger, NY J. Math. **2**, 59 (1996).

[15] W. Jockusch, J. Propp, and P. Shor, e-print math.CO/9801068; H. Cohn, N. Elkies, and J. Propp, Duke. Math. J. **85**, 117 (1996).

[16] H. van Beijeren, Phys. Rev. Lett. **38**, 993 (1977); E. Carlon, G. Mazzeo, and H. van Beijeren, Phys. Rev. B **55**, 757 (1997).